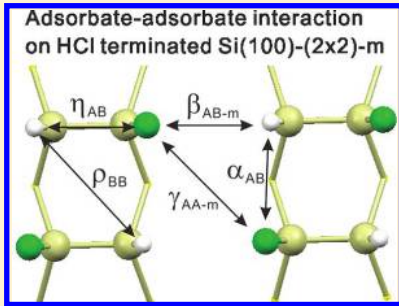


# Energetics and Interactions of Mixed Halogen Adsorbates on the Si(100) Surface

Ying-Hsiu Lin,<sup>†</sup> Hong-Dao Li,<sup>†</sup> Horng-Tay Jeng,<sup>†,‡</sup> and Deng-Sung Lin<sup>\*,†</sup><sup>†</sup>Department of Physics, National Tsing Hua University, 101 Kuang-Fu Road Section Hsinchu 30013, Taiwan<sup>‡</sup>Institute of Physics, Academia Sinica, 128 Sec. 2, Academia Road, Nankang, Taipei 11529, Taiwan

**ABSTRACT:** The energetics of various ordered structures of the Si(100) surface with a 1:1 mixture of two adsorbates (hydrogen–halogen) or (two halogens) are investigated using ab initio density functional theory (DFT) calculations. Through an analysis of the calculated energies of various ordered adsorbate structures, the nearest-neighbor and next-nearest-neighbor interactions between halogen adsorbates are unveiled and observed to fit well with a proposed electron-cloud overlap model. Systematic trends are revealed: The mixing energy of two adsorbates favors desegregated structures. A (2 × 2) structure has the lowest energy on the rectangular Si(100) dimerized surface for all mixed adsorbate systems resulting from the stoichiometric adsorption of diatomic interhalogen molecules and hydrogen halides. These results are in good agreement with the scanning-tunneling microscopy (STM) observations on Si(100) after the adsorption of chlorine-contained molecules HCl and ICl but not for HBr and IBr.



## 1. INTRODUCTION

After impinging upon a surface, a polyatomic molecule often fragments into components that bond with a surface either in close vicinity or at a distance; this process is called dissociative adsorption. An adsorbed component or an adsorbate can not only bond with the substrate but also interact with neighboring adsorbates. The adsorbate–adsorbate interactions, termed AAIs, can occur directly by electrostatic repulsion from their charges<sup>1</sup> or can be indirectly mediated by substrate reconstruction,<sup>2</sup> lattice strain,<sup>3</sup> or surface states.<sup>4,5</sup> AAIs are typically weaker than adsorbate–substrate interactions but can lead to adsorbate orderings or pattern formations on surfaces.<sup>3,6,7</sup> Adsorption of gaseous molecules on solid surfaces is a fundamental process in many natural and technological systems. A comprehensive understanding of AAIs is of great interest to chemical vapor deposition, surface etching, and heterogeneous catalysis.<sup>8</sup>

The physics and chemistry of the Si(100) surface have been extensively studied theoretically and experimentally. The enormous interest in this system stems not only from its rich dangling bond characteristics as a prototype semiconductor surface but also from its important role in semiconductor device fabrication. Due to the crucial role of halogens in silicon chemical etching, the reaction of halogens with the Si(100) surface has been the subject of extensive research.<sup>9–12</sup> To describe the roughening and reorganization experimentally observed on halogen-terminated Si(100) surfaces, Boland et al. performed DFT calculations for selective cells of mixed hydrogen- and halogen-terminated dimers.<sup>7,13–15</sup> They determined the intra-row and inter-row steric repulsions between two neighboring halogen filled dimers.

This work is a sequel to the preceding work on the adsorption of hydrogen halides and diatomic interhalogens on the Si(100) surface.<sup>16</sup> These diatomic molecules are either dissociatively or

abstractively adsorbed at room temperature to yield a mixed-adsorbate surface. STM images show that the mixed hydrogen–chlorine and mixed iodine–chlorine terminated surfaces (Si(100):HCl and Si(100):ICl) consist of local zigzag and (2 × 2) structures.<sup>16,17</sup> Furthermore, the degree of partial orderings is shown to depend on the substrate temperature. Using DFT calculations, the present work examines the energetics of various ordered mixed adsorbate structures. Analyzing the systematic trends of these energies allows the extraction of nearest-neighbor interactions ( $E_{NN}$ ) and next-nearest-neighbor interactions ( $E_{NNN}$ ) between individual adsorbed halogen atoms in the Si(100) surface. The  $E_{NN}$ 's between the two large halogen adsorbates, which include chlorine, bromide, and iodine, are observed to increase exponentially with respect to the sum of their ionic radii. This finding suggests that the steric effect, or the associated cost in energy due to electron-cloud overlap of two adsorbates, contributes predominately to the AAIs and the fragment–adsorbate interactions, which lead to the ordered structure of mixed adsorbates during the chemisorption processes.

## 2. METHODS

**2.1. Computation Details.** Density functional theory (DFT) calculations were performed using VASP (Vienna Ab-initio Simulation Package) employing PBE generalized gradient approximation functionals.<sup>18–21</sup> The Si substrate was modeled by a 4 × 4 × 8 slab with the bottom two layers fixed at bulk positions and the surface terminated by hydrogen. A vacuum region of thickness 15 Å on top of the Si surface was included to form a

**Received:** February 8, 2011

**Revised:** April 29, 2011

**Published:** June 17, 2011

**Table 1.** Atomic Arrangements and Interaction Energies for Mixed Adsorbates A and B in a  $4 \times 4$  Unit Cell on Si(100)<sup>a</sup>

structure i	1: $(2 \times 2)$ -m	2: c( $4 \times 2$ )-m	3: $(2 \times 1)$ -m	4: $(4 \times 1)$ -m	5: c( $4 \times 2$ )-p	6: $(2 \times 2)$ -p	7: $(4 \times 1)$ -p	8: $(2 \times 1)$ -p
atomic	<u>AB AB</u>	<u>AB BA</u>	<u>AB AB</u>	<u>AB BA</u>	<u>AA BB</u>	<u>AA AA</u>	<u>AA BB</u>	<u>AAAA + BBBB</u>
arrange	<u>BA BA</u>	<u>BA AB</u>	<u>AB AB</u>	<u>AB BA</u>	<u>BB AA</u>	<u>BB BB</u>	<u>AA BB</u>	<u>AAAA + BBBB</u>
ment in a	<u>AB AB</u>	<u>AB BA</u>	<u>AB AB</u>	<u>AB BA</u>	<u>AA BB</u>	<u>AA AA</u>	<u>AA BB</u>	<u>AAAA + BBBB</u>
$4 \times 4$ cell	<u>BA BA</u>	<u>BA AB</u>	<u>AB AB</u>	<u>AB BA</u>	<u>BB AA</u>	<u>BB BB</u>	<u>AA BB</u>	<u>AAAA + BBBB</u>
$E_{i,AB}$	$8\eta_{AB}$	$8\eta_{AB}$	$8\eta_{AB}$	$8\eta_{AB}$	$4\eta_{AA} + 4\eta_{BB}$	$4\eta_{AA} + 4\eta_{BB}$	$4\eta_{AA} + 4\eta_{BB}$	$4\eta_{AA} + 4\eta_{BB}$
interaction	$+ 16\alpha_{AB}$	$+ 16\alpha_{AB}$	$+ 8\alpha_{AA}$	$+ 8\alpha_{AA} + 8\alpha_{BB}$	$+ 16\alpha_{AB}$	$+ 16\alpha_{AB}$	$+ 8\alpha_{AA} + 8\alpha_{BB}$	$+ 8\alpha_{AA} + 8\alpha_{BB}$
energy	$+ 8\beta_{AB}$	$+ 4\beta_{AA} + 4\beta_{BB}$	$+ 8\alpha_{BB} + 8\beta_{AB}$	$+ 4\beta_{AA} + 4\beta_{BB}$	$+ 8\beta_{AB}$	$+ 4\beta_{AA} + 4\beta_{BB}$	$+ 8\beta_{AB}$	$+ 4\beta_{AA} + 4\beta_{BB}$
per $4 \times 4$	$+ 8\rho_{AA} + 8\rho_{BB}$	$+ 8\rho_{AA} + 8\rho_{BB}$	$+ 16\rho_{AB}$	$+ 16\rho_{AB}$	$+ 16\rho_{AB}$	$+ 16\rho_{AB}$	$+ 8\rho_{AA} + 8\rho_{BB}$	$+ 8\rho_{AA} + 8\rho_{BB}$
	$+ 8\gamma_{AA} + 8\gamma_{BB}$	$+ 16\gamma_{AB}$	$+ 16\gamma_{AB}$	$+ 8\gamma_{AA} + 8\gamma_{BB}$	$+ 8\gamma_{AA} + 8\gamma_{BB}$	$+ 16\gamma_{AB}$	$+ 16\gamma_{AB}$	$+ 8\gamma_{AA} + 8\gamma_{BB}$
$E_i = E_{i,AH} -$	$-E'_0$	$-E'_0$	$-E'_0$	$-E'_0$				0
$E_{8,AH}$	$-8\alpha_{AA} - 4\beta_{AA}$	$-8\alpha_{AA}$	$-4\beta_{AA}$		$-8\alpha_{AA} - 4\beta_{AA}$	$-8\alpha_{AA} - 8\rho_{AA}$	$-4\beta_{AA}$	
		$-8\gamma_{AA}$	$-8\rho_{AA} - 8\gamma_{AA}$	$-8\rho_{AA}$	$-8\rho_{AA}$	$-8\gamma_{AA}$	$-8\gamma_{AA}$	
$E_{i,\text{est}}$	$-E'_0 - 12E_{NN}$	$-E'_0 - 8E_{NN}$	$-E'_0 - 4E_{NN}$	$-E'_0$	$-12E_{NN}$	$-8E_{NN}$	$-4E_{NN}$	0

<sup>a</sup> The energy for  $(2 \times 1)$ -p,  $E_{8,AB}$ , is the mean of the two energies for A- and B-terminated  $(2 \times 1)$  structure, respectively. With B = H, energy  $E_i$  is relative to  $E_{8,AH}$ .  $E_{NN}$  denotes the energy of the nearest-neighbor interaction  $\alpha_{AA}$  or  $\beta_{AA}$  assuming  $\alpha_{AA} \approx \beta_{AA}$ .  $E_{i,\text{est}}$  represents an estimation of  $E_i$  by neglecting  $E_{NNN}$ 's  $\rho_{AA}$ 's and  $\gamma_{AA}$ 's.

supercell. Plane waves of kinetic energies up to 25 Ry were included. The irreducible Brillouin zone was sampled with a  $(16 \times 16 \times 1)$  Monkhorst–Pack mesh.<sup>22</sup> Geometry optimization was performed until the total energy converged to within  $10^{-5}$  eV. Cell sizes were fixed to yield a Si lattice constant of 5.46 Å. After a relaxation of the atomic structure, electronic densities of states calculations were performed. STM images were simulated using the Tersoff and Hamann approximation that relates the STM image to the integrated electronic density of states between the Fermi level and the bias voltage.<sup>23</sup> We simulate a constant-height mode STM image by integrating the partial charge density from  $E_F$  to  $E_F \pm 2.0$  eV onto a projected plane at a distance of 2.3 Å above the topmost atom on the surface.

**2.2. Steric Interaction Model.** The Si(100) surface consists of dimers; each surface dimer atom has a chemically active dangling bond.<sup>24</sup> Since both H and the halogen atom X are highly reactive radicals, the reaction of hydrogen halides HX and diatomic interhalogens XY with Si(100) involves dissociative adsorption with each H radical and halogen atom forming a single bond concurrently with two partially filled dangling bonds through the cleavage of the H–X or X–Y bond.<sup>17,25,26</sup> After saturation coverage, the surface became fully terminated with the mixed (H–Si and X–Si) or (X–Si and Y–Si) surface species as observed by photoemission and STM. The dimer bonds remained intact after surface passivation by hydrogen or halogen atoms.

To describe the ordered adsorbate structures that are possible for two adsorbates, the following symbols are introduced: the two possible adsorbates, either hydrogen and halogen atoms or two halogen atoms, are denoted by A and B, respectively. The basic building blocks for the Si(100):AB surface are mixed occupation dimers (MOD) A–Si–Si–B (AB for short) or B–Si–Si–A (BA) or paired occupation dimers (POD) A–Si–Si–A (AA) or B–Si–Si–B (BB). Using this notation, the various ordered adsorbate structures in a  $4 \times 4$  cell can be represented schematically as shown in Table 1. Eight different periodic structures were considered: (1)  $(2 \times 2)$ -m, (2) c( $4 \times 2$ )-m, (3)  $(2 \times 1)$ -m, (4)  $(4 \times 1)$ -m, (5) c( $4 \times 2$ )-p, (6)  $(2 \times 2)$ -p, (7)  $(4 \times 1)$ -p, and (8)  $(2 \times 1)$ -p, where m and p indicate that the structure is formed only by MODs and PODs, respectively. The

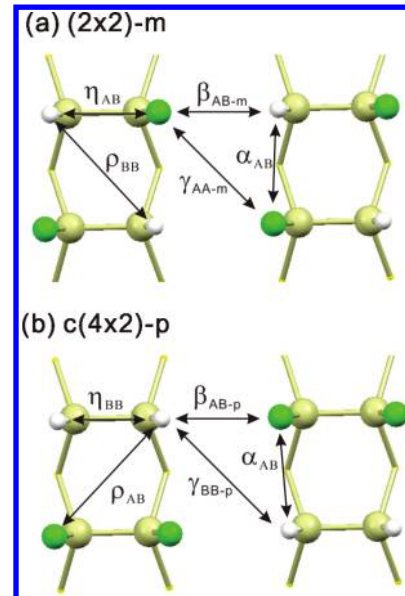


**Figure 1.** Top view of half of the (a)  $(2 \times 2)$ -m and (b) c( $4 \times 2$ )-p unit cell used to calculate adsorbate–adsorbate interactions.  $\eta$ ,  $\alpha$ , and  $\beta$  represent the interactions between two nearest-neighboring adsorbate atoms of the same kind (A or B) or different kinds (A and B). Those between two next-nearest neighbors are labeled as  $\rho$  and  $\gamma$ .

$(2 \times 1)$ -p structure describes a surface where the top half is Si(100)-(2  $\times$  1):A and the bottom half is Si(100)-(2  $\times$  1):B.

Several fundamental AAs are depicted in Figure 1:  $\eta_{AB}$ , the chemical and steric interaction between two adsorbate atoms A and B in a dimer;  $\alpha_{AB}$ ,  $E_{NN}$  between two adsorbate atoms A and B in two neighboring dimers in the same row;  $\beta_{AB}$ ,  $E_{NN}$  between two adsorbate atoms A and B in two neighboring rows;  $\rho_{AB}$ ,  $E_{NNN}$  between two adsorbate atoms A and B in the same dimer row; and  $\gamma_{AB}$ ,  $E_{NNN}$  between two adsorbate atoms A and B in neighboring dimers in the same row. Accordingly, each of the total adsorbate–adsorbate interaction energies  $E_{i,AB}$  for the above-mentioned  $i$ th structure are also listed in Table 1.

Within a POD or a MOD, charge transfer, and thereby the bond strength of Si–A or Si–B at one end of the dimer, can be affected by the adsorbate at the other end. Hence, the interactions within a dimer ( $\eta_{AB}$ ,  $\eta_{AA}$ , and  $\eta_{BB}$ ) include not only AAIs but also chemical energies that involve the formations of A–Si–Si–B, A–Si–Si–A, and B–Si–Si–B. To extract the AAIs, we can exclude these chemical energy components using a relative energy scale  $E_i$  for the  $i$ th structure to  $E_{8,AB}$  ( $= 0$ ). To further reduce the number of terms in the interactions, hydrogen can be used as the adsorbed atoms B because the interaction between hydrogen and halogen adsorbate atoms is negligible:  $\pi_{HH} = \pi_{AH} = 0$ , where  $\pi = \eta$ ,  $\alpha$ ,  $\beta$ ,  $\rho$ , or  $\gamma$ , and A = halogen. With these simplifications, the relative interaction energies  $E_i$  for the mixed hydrogen–halogen terminated surfaces Si(100):HA are as follows.

$$E_1 = -E_0' - 8\alpha_{AA} - 4\beta_{AA} \quad (m1)$$

$$E_2 = -E_0' - 8\alpha_{AA} - 8\gamma_{AA} \quad (m2)$$

$$E_3 = -E_0' - 4\beta_{AA} - 8\rho_{AA} - 8\gamma_{AA} \quad (m3)$$

$$E_4 = -E_0' - 8\rho_{AA} \quad (m4)$$

$$E_5 = -8\alpha_{AA} - 4\beta_{AA} - 8\rho_{AA} \quad (p1)$$

$$E_6 = -8\alpha_{AA} - 8\rho_{AA} - 8\gamma_{AA} \quad (p2)$$

$$E_7 = -4\beta_{AA} - 8\gamma_{AA} \quad (p3)$$

$$E_8 = 0 \quad (p4)$$

Note that the chemical and steric interactions in a dimer are grouped in the term:  $E_0' = 4\eta_{AA} + 4\eta_{HH} - 8\eta_{AH}$ . The variable  $E_0'$  in eqs m1–m4 can be eliminated by subtraction; the AAIs are then derived as

$$\beta_{AA-m} = (-E_1 + E_2 - E_3 + E_4)/8 \quad (m5)$$

$$\gamma_{AA-m} = (E_1 - E_2 - E_3 + E_4)/16 \quad (m6)$$

$$\alpha_{AA} - \rho_{AA} = (-E_1 - E_2 + E_3 + E_4)/16 \quad (m7)$$

In eqs m5 and m6, an additional label m is added to the interaction energies  $\beta$ 's and  $\gamma$ 's because the  $\beta$ 's and  $\gamma$ 's can be similarly derived independently of eqs p1–p4 for the POD configurations

$$\beta_{AA-p} = (-E_5 + E_6 - E_7 + E_8)/8 \quad (p5)$$

$$\gamma_{AA-p} = (E_5 - E_6 - E_7 + E_8)/16 \quad (p6)$$

$$\alpha_{AA} + \rho_{AA} = (-E_5 - E_6 + E_7 + E_8)/16 \quad (p7)$$

The bond angle and charge distribution for a Si–X bond in an MOD are expected to be slightly different from those in a POD (see Section 3.1). Therefore, it is expected that  $\beta_{AA-m}$  ( $\gamma_{AA-m}$ ) is different from  $\beta_{AA-p}$  ( $\gamma_{AA-p}$ ). Equations m7 and p7 are used to obtain a set of  $\alpha_{AA}$  and  $\rho_{AA}$

$$\alpha_{AA} = (-E_1 - E_2 + E_3 + E_4 - E_5 - E_6 + E_7 + E_8)/32 \quad (8)$$

$$\rho_{AA} = (E_1 + E_2 - E_3 - E_4 - E_5 - E_6 + E_7 + E_8)/32 \quad (9)$$

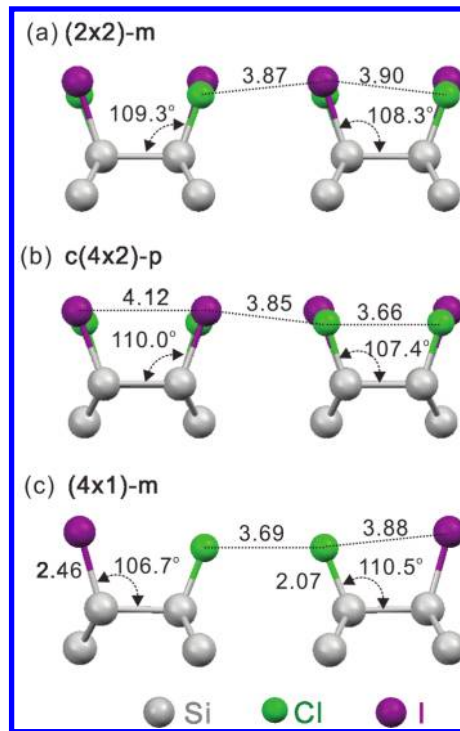


**Figure 2.** Side view of relaxed (a)  $(2 \times 2)$ -m, (b)  $c(4 \times 2)$ -p, and (c)  $(4 \times 1)$ -m atomic structure of the ICl-terminated Si(100) surface. The atomic distance is in angstrom. The bond lengths of Si–Cl (2.07 Å) and Si–I (2.46 Å) are almost equal for all structures.

### 3. RESULTS AND DISCUSSION

**3.1. Relaxed Structure and Simulated STM Images of ICl/Si(100).** Saturation adsorption of monovalent adatoms such as H or halogen on the Si(100) surface results in termination of all dangling bonds.<sup>24,27</sup> In good agreement with earlier calculations,<sup>28</sup> we determine a surface dimer bond length of 2.41 Å and a dimer tilt angle of 111° for the hydrogen-terminated Si(100) surface (Si(100)-(2 × 1):H). The structural data calculated for Si(100)-(2 × 1):Cl, a Si–Cl bond length of 2.07 Å, and a dimer length of 2.43 Å are also in close agreement with previous results.<sup>29,30</sup>

As Figure 2 shows, the calculated relaxed geometric parameters for Si(100):AB are similar for various ordered structures. Taking mixed adsorbate atoms I and Cl, for example, the bond lengths of Si–Cl and Si–I are 2.07 and 2.46 Å, respectively. Under the influence of neighboring adsorbates, the Si–I and Si–Cl bond angles with respect to the dimer bond vary slightly, as depicted in Figure 2. As described in Section 3.4, the AAIs are repulsive due to the electron-cloud overlap between the two neighboring adsorbates. Because the large halogen adsorbate ions have large electron clouds, the bond angles are optimized such that the overall overlap energy is minimized.

Even though each halogen or hydrogen atom similarly terminates one dangling bond, previous reports have shown that chemical contrast between different Si–X sites in STM images is high.<sup>16</sup> In fact, only one of the two adsorbates for Si(100):AB is discernible in the STM images. Simulation of STM images for the mixed adsorbate systems can help to identify the type of halogens that have a relatively larger apparent height. Figures 3(a) and 3(b) show the simulated constant-height STM images of the ICl-terminated Si(100)-(2 × 2)-m surface (Figures 3(c) and 3(d)). The simulation was obtained by integrating the DOS from  $E_F$  to

$E_F \pm 2.0$  eV onto a projected plane at 2.3 Å above iodine. According to Figure 3(a), the bright protrusions in the empty-state STM image should be assigned to the iodine atoms.

**3.2. Calculated Adsorbate–Adsorbate Energy.** The adsorption energies for various hydrogen halides HX and diatomic interhalogens XY on the Si(100)-(2 × 1) structure are listed in Table 2. The calculated relative energies  $E_i$  for mixed hydrogen–halogen adsorbates are obtained by subtracting  $E_{ad,8}$  from  $E_{ad,i}$  and displayed in Figure 4. Giving the calculated  $E_i$ 's and solving eqs m5, m6, p5, p6, 8, and 9 in Section 2.2 yield the interaction energies, which are listed in Table 3. From Table 3, the next-nearest-neighbor interactions  $E_{NNN}$  are seen to be similarly weak for all halogens, consistent with previous

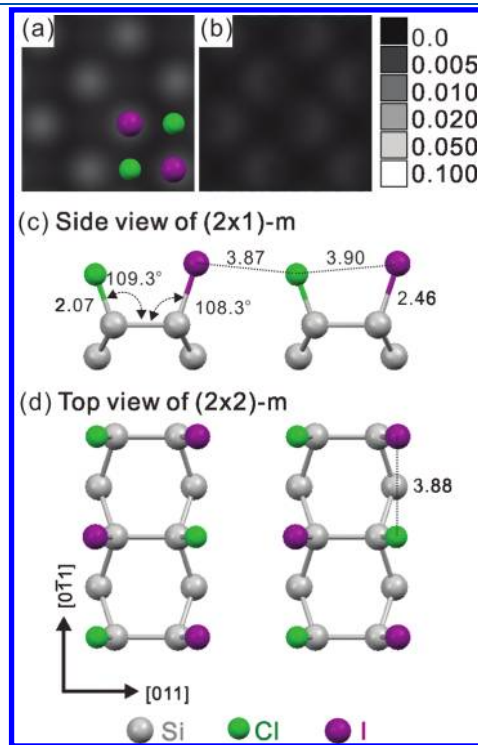


**Figure 3.** Calculated constant-height (a) empty-state and (b) filled-state STM images of the (2 × 2)-m adsorbate structure for Si(100):ICl. The electron density is in units of  $e/\text{\AA}^3$ . The maxima of electron density are at the iodine positions. (c) Side view and (d) top view of the relaxed atomic structure of a (2 × 1)-m ICl-terminated Si(100) surface. The distance is in angstrom.

reports.<sup>13</sup> Independent of reactivity and the amount of charge transferred to the various halogens,  $E_{NNN}$  are likely associated with strains in the top Si layer. The magnitudes of the interactions between nearest-neighbors  $E_{NN}$  are in overall agreement with those found in ref 13 and will be further discussed in Section 3.3.

The energy diagram in Figure 4 shows several analogous trends for the four hydrogen halides:

1.  $E_8$  has the highest value among the eight  $E_i$ 's. Accordingly, the segregation into the hydrogen- and halogen-terminated domains is not energetically favorable, even when it is kinetically plausible.
2. The total energies are in the same order from lowest to highest:  $E_1 < E_2 < E_3 < E_4$  for the MOD configurations, and  $E_5 < E_6 < E_7 < E_8$  for the POD configurations. Furthermore, the relative energies ( $E_1, E_2, E_3, E_4$ ) for the MOD configurations and those ( $E_5, E_6, E_7, E_8$ ) for the POD configurations are about equally spaced for all the H–Cl, H–Br, and H–I mixed adsorbate systems. As the estimated total energies  $E_{i,\text{est}}$ 's in Table 1 show, the gap in total energy is about  $4E_{NN}$  when the  $E_{NNN}$ 's are set to zero and the nearest-neighbor interaction  $\alpha$ 's and  $\beta$ 's are set equal,  $\alpha = \beta = E_{NN}$ . In the H–F system, all structures have comparable energies, apart from the segregated structure (2 × 1)-p. The  $E_{NNN}$ 's between the two F adsorbate atoms are comparable with the  $E_{NN}$ 's and, therefore, cannot be ignored in the estimation of the total energies.
3. The energy of (4 × 1)-m is lower than that of (2 × 1)-p, which implies that  $E'_0 = 4\eta_{XX} + 4\eta_{HH} - 8\eta_{XH} > 0$  or equivalently  $\eta_{XX} + \eta_{HH} > 2\eta_{XH}$ . In other words, the formation of two MODs HX upon chemisorption of two HX molecules is energetically preferable to that of two different PODs XX and HH.
4. The (2 × 2)-m and c(4 × 2)-p orderings have the lowest total energies for the MOD and POD configurations, respectively. Although their energies are compatible, the c(4 × 2)-p ordering has not yet been observed.<sup>16</sup> This occurrence indicates that the thermodynamic consideration alone is not sufficient to determine the adsorbate structure and that the kinetic barrier comes into play. Take the HCl adsorption as an example. The MODs (H–Si–Si–Cl) are the dominating species on 1D and 2D arrays of bare Si dimers.<sup>31</sup> At low coverages, bare dimers (–Si–Si–) are abundant. A previous study suggests that, upon the adsorption of a HCl molecule on a bare dimer, an intermediate state (–Si–Cl–Si–H) with Cl inserted

**Table 2. Calculated Adsorption Energies (meV per (4 × 4) cell),  $E_{ad,i}$  with the  $i$ th Adsorption Structure for Eight Diatomic HX/XY Molecules on Si(100)**

structure $i$	1: (2 × 2)-m	2: c(4 × 2)-m	3: (2 × 1)-m	4: (4 × 1)-m	5: c(4 × 2)-p	6: (2 × 2)-p	7: (4 × 1)-p	8: (2 × 1)-p
HF	−24521.2	−24496.2	−24479.7	−24400.8	−24463.4	−24446.4	−24387.3	−24241.1
HCl	−22354.0	−22283.5	−22160.0	−22046.1	−22368.5	−22311.0	−22133.7	−21998.8
HBr	−22910.7	−22763.5	−22543.4	−22361.1	−22923.5	−22757.9	−22509.1	−22263.7
HI	−22926.0	−22555.8	−21969.3	−21590.6	−22936.4	−22291.9	−21934.5	−21208.2
ClF	−53720.5	−53693.5	−53671.7	−53633.3	−53719.3	−53672.5	−53659.9	−53601.7
BrF	−49316.9	−49220.2	−49143.6	−49026.9	−49310.7	−49141.8	−49114.6	−48929.4
IF	−42296.6	−42030.5	−41602.1	−41314.2	−42252.3	−41630.7	−41568.9	−40863.3
BrCl	−38552.5	−38539.7	−38519.4	−38505.4	−38548.9	−38521.1	−38514.9	−38483.7
ICl	−33735.7	−33659.9	−33380.2	−33285.3	−33705.7	−33404.1	−33346.5	−33029.8
IBr	−30700.7	−30662.9	−30510.4	−30467.7	−30668.4	−30522.6	−30488.4	−30340.5

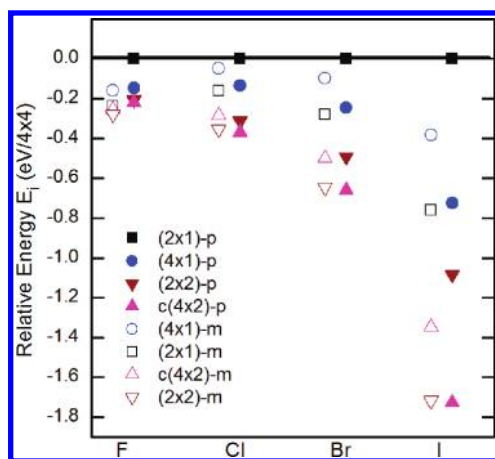


**Figure 4.** Relative energy  $E_i$  for mixed hydrogen- and halogen-terminated Si(100) surfaces in various adsorbate structures as labeled. Energies refer to that of the  $(2 \times 1)$ -p structure, which is set to zero.

**Table 3. Calculated Interaction Energies,  $E_{NN}$ 's and  $E_{NNN}$ 's, Respectively, between Two Nearest Neighbors and Two Next Nearest Neighbors of the Same Kind (A)<sup>a</sup>**

	energy (meV)	AA = FF	AA = ClCl	AA = BrBr	AA = II
$E_{NN}$	$\alpha_{AA}$	13.1 (12)	30.6 (30.5)	52.4 (53)	125.2 (75)
	$\beta_{AA-m}$	13.0	23.1	41.2	93.6
	$\beta_{AA-p}$	20.4 (14)	24.1 (26)	51.4 (52)	171.4 (75)
$E_{NNN}$	$\rho_{AA}$	4.5	3.6	4.3	5.1
	$\gamma_{AA-m}$	3.4	2.7	2.2	0.5
	$\gamma_{AA-p}$	8.1	4.8	5.0	5.1

<sup>a</sup> See text for details. Data in the parentheses are from refs 13 (for FF, ClCl, and BrBr) and 32 (for II). Note that the  $\alpha$  interaction in ref 13 is between two neighboring dimers and is, therefore, equal to  $2\alpha_{AA}$  herein.

between two Si atoms is formed. This bridge-bonded Cl intermediate state mostly further relaxes into a MOD.<sup>31</sup> At higher coverages, some singly occupied dimers are ( $-\text{Si}-\text{Si}-\text{Cl}$ ) present due to abstractive adsorption. It was found that the adsorbed Cl atom on one side of a bare dimer effectively hampers the adsorption of a second dissociated Cl radical on the other side.<sup>17</sup> The effective repulsion between a Cl adsorbate and a Cl radical reduces the formation probability of PODs ( $\text{H}-\text{Si}-\text{Si}-\text{H}$  and  $\text{Cl}-\text{Si}-\text{Si}-\text{Cl}$ ), again hindering the formation of the  $c(4 \times 2)$ -p adsorbate structure.

**3.3. Interaction between Halogen Adsorbates.** The calculated energies  $E_{i,AB}$  for mixed halogen adsorbates A (= X) and B (= Y) are shown in Figure 5. In contrast with the mixed H- and X-terminated surface, all interactions between the same adsorbates ( $\pi_{XX}$  and  $\pi_{YY}$ ) or between two adsorbates X and Y,  $\pi_{XY}$ , need to be included in the calculations. However, several similarities in the energy trend of various structures are still evident in Figure 5:

1.  $E_{8,XY}$ , expressed concisely in this section as  $E_{(2 \times 1)-p}$ , is the highest one among the eight structures, suggesting that two adsorbates prefer to mix.
2. The total energies are in the same order from lowest to highest:  $E_{(2 \times 2)-m} < E_{c(4 \times 2)-m} < E_{(2 \times 1)-m} < E_{(4 \times 1)-m}$  for the MOD configurations and  $E_{c(4 \times 2)-p} < E_{(2 \times 2)-p} < E_{(4 \times 1)-p} < E_{(2 \times 1)-p}$  for the POD configurations. The energy difference

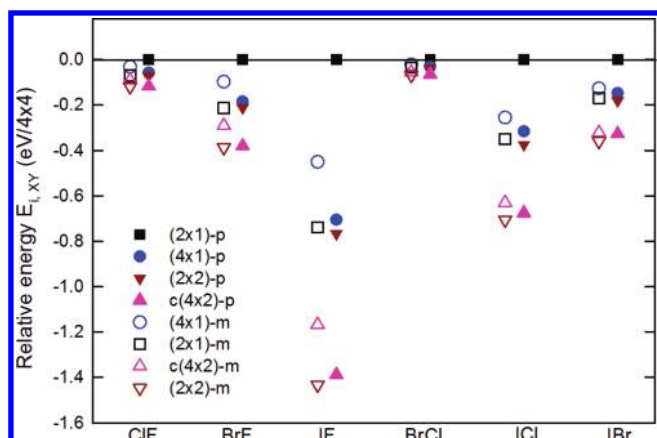


**Figure 5.** Relative energy  $E_{i,XY}$  for Si(100) saturated with mixed halogen atoms X and Y in various adsorbate structures as labeled. Energies are referred to that of the  $(2 \times 1)$ -p structure.

between  $E_{c(4 \times 2)-m}$  and  $E_{(2 \times 2)-m}$ ,  $\Delta E_m$ , is comparable to that between  $E_{(4 \times 1)-m}$  and  $E_{(2 \times 1)-m}$ . Similarly, the energy difference between  $E_{(2 \times 2)-p}$  and  $E_{c(4 \times 2)-p}$ ,  $\Delta E_p$ , is almost equal to that between  $E_{(2 \times 1)-p}$  and  $E_{(4 \times 1)-p}$ . Analyzing  $E_{i,AB}$  in Table 1 and neglecting the small  $E_{NNN}$ 's yields  $\Delta E_m \approx 4\beta_{AA-m} + 4\beta_{BB-m} - 8\beta_{AB-m}$  and  $\Delta E_p \approx 4\beta_{AA-p} + 4\beta_{BB-p} - 8\beta_{AB-p}$ .

3. The energy of  $(4 \times 1)$ -m is lower than that of  $(2 \times 1)$ -p, again suggesting that the formation of two MODs XY upon chemisorption of two XY molecules is energetically more desirable than that of two different POD XX and YY.
4. The  $(2 \times 2)$ -m and  $c(4 \times 2)$ -p structures have the lowest interaction energies for the MOD and POD configurations, respectively. In the ICl case, only the  $(2 \times 2)$ -m structure is observed,<sup>16</sup> although the energies of the two structures are comparable. Because of the pairing energy between the two dangling bonds on a dimer, the formation of a MOD XY on a bare dimer upon the adsorption of XY is energetically more favorable than that of two singly occupied dimers. However, the energy gain in the formation of an individual MOD upon each XY adsorption cannot explain the formation of large  $(2 \times 2)$ -m patches, in which neighboring MODs have alternating orientations. In sharp contrast to the Si(100):ICl surface, no apparent ordered structure is observed on the Si(100):IBr surface.<sup>16</sup> Therefore, the energy factor alone is not sufficient for the formation of an ordered mixed halogen structure. A previous study has reported the importance of a long-lived intermediate state during the adsorption of HCl.<sup>31</sup> The intermediate state involves a bridge-bonded Cl configuration. In this intermediate picture, the lifetime of the intermediate state is sufficiently long for the second incoming XCl or HCl to sense the strain, electrostatic, or steric effects from the adsorption configuration of its neighbors and adopt the apparently more favorable zigzag arrangement. The absence of an ordered structure for Si(100):IBr and Si(100):HBr can be attributed to the lack of the intermediate state since Br or I is chemically less active than Cl.

Following the same method presented in Section 2.2, the equations for  $E_{i,AB}$  can be solved by applying the interactions shown in Table 3. Three nearest-neighbor interactions and three next-nearest-neighbor interactions are found and listed in

**Table 4. Calculated Interaction Energies (meV) between Two Different Kinds of Halogen Adsorbate Atoms<sup>a</sup>**

energy	AB =	ClF	BrF	IF	BrCl	ICl	IBr
$E_{NN}$	$\alpha_{AB}$	18.1	20.6	24.4	39.3	55.0	77.2
	$\beta_{AB-m}$	13.9	13.8	18.7	30.4	47.7	62.4
	$\beta_{AB-p}$	15.7	13.8	12.9	34.0	59.1	93.0
$E_{NNN}$	$\rho_{AB}$	3.7	3.8	4.2	3.9	4.3	5.1
	$\gamma_{AB-m}$	2.7	2.2	1.3	2.4	1.0	1.2
	$\gamma_{AB-p}$	6.1	6.0	4.0	4.8	4.5	5.0

<sup>a</sup> See the text for details.

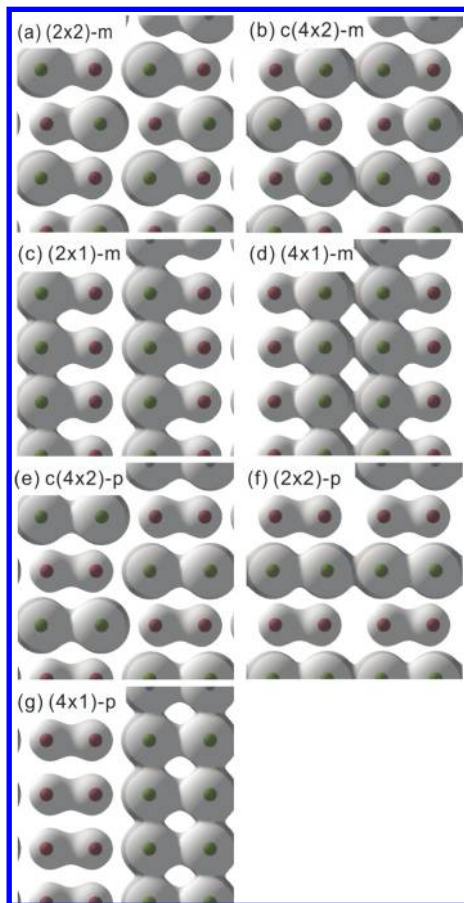


**Figure 6.** Charge density distributions of seven nonsegregated ordered structures of mixed hydrogen (dark red) and iodine (green) atoms with the same charge density iso-surface ( $0.028 \text{ e}/\text{\AA}^3$ ) are indicated.

Table 4. Again, the  $E_{NNN}$ 's are relatively small and show no obvious trends for the various halogens; they are not directly related to AAIs but more likely to the lattice strain energy. Except for the  $\beta$ 's involving fluorine, the energy  $\alpha_{AB}$  ( $\beta_{AB}$ ) lies between  $\alpha_{AA}$  and  $\alpha_{BB}$  ( $\beta_{AA}$  and  $\beta_{BB}$ ) and is less than the mean of the two. These and other observations are further discussed in Section 3.4.

**3.4. Origin of the Interactions.** In Tables 3 and 4, the calculated interaction energies between two adsorbed halogen atoms apparently rise with increasing atomic numbers. Since larger halogen atoms cause less charge transfer from the surface Si upon termination, the electrostatic or Madelung energy between ions ( $X^-$  or  $\text{Si}^+$ ) cannot account for the trend. The ionic radius of chlorine

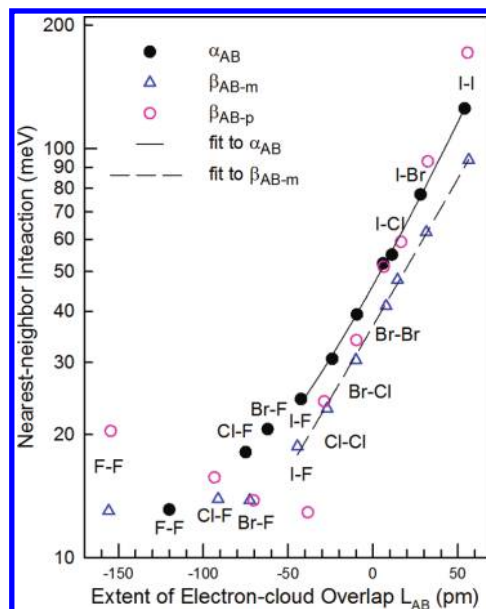


**Figure 7.** Nearest-neighbor interactions vs the extent of electron-cloud overlap between two halogen adsorbates A and B as labeled.

(181 pm) is about equal to half of the ( $1 \times 1$ ) lattice constant ( $a = 386 \text{ pm}$ ) of the unreconstructed  $\text{Si}(100)$  surface, while those of bromide and iodine (196 and 220 pm) are markedly larger than  $a/2$ . Therefore, the electron clouds of two neighboring adsorbed halogen atoms, except F atoms, overlap. Hence, the increasing interaction energy of the systems can be attributed to Coulomb exclusion.

To further understand the driving force behind the ordered structure observed experimentally and the striking features and tendencies mentioned above, we plot the charge distributions to illustrate the adsorbate–adsorbate interactions. Figure 6 shows the charge density distribution of seven nonsegregated ordered structures consisting of H and I with the same iso-surface. Visual inspection of the figures suggests that ( $2 \times 2$ )-m and c( $4 \times 2$ )-p have the least amount of electron-cloud overlap among the MOD and POD structures, respectively. With the least amount of electron-cloud overlap, the ( $2 \times 2$ )-m pattern thereby has the lowest total energy and results in the most stable pattern. Among various MOD configurations, the extent of electron-cloud overlap (from least to most) is ( $2 \times 2$ )-m, c( $4 \times 2$ )-m, ( $2 \times 1$ )-m, and ( $4 \times 1$ )-m, in the same order as the total energies in Figure 4. Figures 6 and 4 also show that the extent of electron-cloud overlap for the POD arrangements corresponds well with their total energies, too.

In the ionic solids or crystals of inert gases, the repulsive energy due to the electron-cloud overlap between two neighboring atoms can often be expressed empirically in an exponential form  $\lambda \exp(L_{AB}/\rho)$ , where  $\lambda$  is a potential parameter,  $\rho$  is a measure of the interaction range, and  $L_{AB}$  is a measure of the extent of electron-cloud overlap between halogen adsorbates A and B. Figure 7 displays the nearest-neighbor interaction  $E_{NN}$  as a function of the extent of electron-cloud overlap  $L_{AB} = R_A + R_B - d_{AB}$ , where  $R_A$  and  $R_B$  are the ionic radii of the two interaction halogen atoms A and B, respectively, and  $d_{AB}$  is the calculated internuclear distance between A and B. As Figure 7 displays,  $L_{BrBr} \approx 0$  and  $L_{AF} \ll 0$ . The  $d_{AB}$ 's and the resultant  $L_{AB}$ 's along (for  $\alpha_{AB}$ ) and across (for  $\beta_{AB}$ ) the dimer row vary only slightly (within about 5 pm), except for those involving fluorine because of its small ionic radius. On a logarithmic

scale,  $\alpha$ 's and  $\beta$ 's are proportional to  $L_{AB}$  over the range  $-50$  to  $50$  pm, suggesting that the exponential form is appropriate. The calculated optimal fitting functions are  $\alpha_{AB} = 7.8 + 38.4 \times \exp(L_{AB}/48.3)$ ,  $\beta_{AB-m} = 7.2 + 36.1 \times \exp(L_{AB}/59.56)$ , and  $\beta_{AB-p} = 10.2 + 32.1 \times \exp(L_{AB}/34.5)$ . The common offsets of around  $10$  meV can be attributed to the substrate strain energy because the relatively small amount of energy persists for nonoverlapping halogen adsorbates such as A (= F, Cl, Br) and F. The differences in the potential parameters  $\lambda$  are within  $\sim 15\%$ ; the interaction range also varies with the type of interactions. These variations may be attributed in part to the nonspherical electron clouds at the halogen end in a partial ionic Si–X bond.

#### 4. CONCLUSION

The dissociative adsorption of diatomic molecules or coadsorption of two gases on a surface can produce an overlayer that consists of mixed adsorbates. We have performed comprehensive DFT calculations and analysis of eight ordered adsorbate structures for the mixed hydrogen- and/or halogen-terminated Si(100) surface. The sizes of adsorbate halogen ions and the ionicity of the Si–X bonds vary greatly, yet similar trends are identified for the various mixtures: The energies of the eight structures are in the same order. The segregated structure has the highest energy, and the  $(2 \times 2)$ -m has the lowest. An analysis of the energies of the eight types of mixed adsorbate structures also produces several nearest-neighbor interactions  $E_{NN}$  between similar or dissimilar halogen adsorbates on the Si(100) surface.  $E_{NN}$ 's are observed to rise exponentially with the extent of electron-cloud overlap between two neighboring adsorbate atoms, thereby suggesting that the origin of the adsorbate–adsorbate interactions on the halogen-covered Si(100) is steric. The findings herein are likely applicable to other surface–adsorbate/mixed adsorbate systems.

#### ■ AUTHOR INFORMATION

##### Corresponding Author

\*E-mail: dslin@phys.nthu.edu.tw.

#### ■ ACKNOWLEDGMENT

The authors wish to acknowledge the financial support of Taiwan's National Science Council under grant NSC 99-2119-M-007-005-MY3 (DSL). We are grateful to the National Center for High-Performance Computing of Taiwan for providing computational support.

#### ■ REFERENCES

- (1) Rockey, T. J.; Yang, M.; Dai, H.-L. *J. Phys. Chem. B* **2006**, *110*, 19973.
- (2) Brihuega, I.; Cano, A.; Ugeda, M. M.; Saenz, J. J.; Levanyuk, A. P.; Gomez-Rodriguez, J. M. *Phys. Rev. Lett.* **2007**, *98*, 156102.
- (3) Österlund, L.; Pedersen, M. O.; Stensgaard, I.; Læsgaard, E.; Besenbacher, F. *Phys. Rev. Lett.* **1999**, *83*, 4812.
- (4) Bogicevic, A.; Ovesson, S.; Hyldgaard, P.; Lundqvist, B. I.; Brune, H.; Jennison, D. R. *Phys. Rev. Lett.* **2000**, *85*, 1910.
- (5) Hyldgaard, P.; Persson, M. *J. Phys.: Condens. Matter* **2000**, *12*, L13.
- (6) Zhdanov, V. P. *Langmuir* **2001**, *17*, 1793.
- (7) Chen, D.; Boland, J. J. *Phys. Rev. Lett.* **2004**, *92*, 096103.
- (8) Somorjai, G. A. *Introduction to Surface Chemistry and Catalysis*; John Wiley & Sons: New York, 1994.
- (9) Winters, H. F.; Coburn, J. W. *Surf. Sci. Rep.* **1992**, *14*, 162.
- (10) Boland, J. J.; Weaver, J. H. *Phys. Today* **1998**, *51*, 34.
- (11) Aldao, C. M.; Weaver, J. H. *Prog. Surf. Sci.* **2001**, *68*, 189.
- (12) Chander, M.; Goetsch, D. A.; Aldao, C. M.; Weaver, J. H. *Phys. Rev. Lett.* **1995**, *74*, 2014.
- (13) Herrmann, C. F.; Chen, D.; Boland, J. J. *Phys. Rev. Lett.* **2002**, *89*, 096102.
- (14) Chen, D.; Boland, J. J. *Phys. Rev. B* **2003**, *67*, 195328.
- (15) Chen, D.; Boland, J. J. *Phys. Rev. B* **2004**, *70*, 205432.
- (16) Hou, H.-Y.; Wu, H.-H.; Chung, J.-Y.; Lin, D.-S. *J. Phys. Chem. C* **2011**, *115*, 13268–13274.
- (17) Hsieh, M.-F.; Cheng, J.-Y.; Yang, J.-C.; Lin, D.-S.; Morgenstern, K.; Pai, W.-W. *Phys. Rev. B* **2010**, *81*, 045324.
- (18) Blöchl, P. E. *Phys. Rev. B* **1994**, *50*, 17953.
- (19) Kresse, G.; Joubert, D. *Phys. Rev. B* **1999**, *59*, 1758.
- (20) Perdew, J. P.; Burke, K.; Ernzerhof, M. *Phys. Rev. Lett.* **1996**, *77*, 3865.
- (21) Kresse, G. *Phys. Rev. B* **2000**, *62*, 8295.
- (22) Monkhorst, H. J.; Pack, J. D. *Phys. Rev. B* **1976**, *13*, 5188.
- (23) Tersoff, J.; Hamann, D. R. *Phys. Rev. B* **1985**, *31*, 805.
- (24) Boland, J. J. *Adv. Phys.* **1993**, *42*, 129.
- (25) Waltenburg, H. N.; Yates, J. T. *Chem. Rev.* **1995**, *95*, 1589.
- (26) Ferng, S.-S.; Wu, S.-T.; Lin, D.-S.; Chiang, T. C. *J. Chem. Phys.* **2009**, *130*, 164706.
- (27) Boland, J. J. *Science* **1993**, *262*, 1703.
- (28) Wang, N.-P.; Rohlfing, M.; Krüger, P.; Pollmann, J. *Phys. Rev. B* **2006**, *74*, 155405.
- (29) Lee, J. Y.; Kang, M.-H. *Phys. Rev. B* **2004**, *69*, 113307.
- (30) de Wijs, G. A.; De Vita, A.; Selloni, A. *Phys. Rev. B* **1998**, *57*, 10021.
- (31) Li, H.-D.; Chang, C.-Y.; Chien, L.-Y.; Chang, S.-H.; Chiang, T. C.; Lin, D.-S. *Phys. Rev. B* **2011**, *83*, 075403.
- (32) Zarkevich, N. A.; Johnson, D. D. *Surf. Sci.* **2005**, *591*, L292.